An Iterative Matrix-Free Method in Implicit Immersed Boundary/Continuum Methods

X. Sheldon Wang

Department of Mathematical Sciences
New Jersey Institute of Technology
Newark, NJ 07102

CAMS Report 0607-21, Spring 2007

Center for Applied Mathematics and Statistics

NJIT

1 Abstract

The objective of this paper is to present an iterative solution strategy for implicit immersed boundary/continuum methods. An overview of the newly proposed immersed continuum method in conjunction with the traditional immersed boundary method will also be presented. As a key ingredient of the fully implicit time integration, a matrix-free combination of Newton-Raphson iteration and GMRES iterative linear solver is proposed.

2 Introduction

For the past decades, significant efforts have been drawn to the development of computational tools for fluid-structure interaction (FSI) analysis [17] [18] [20] [43]. The immersed boundary method was initially developed by Peskin, 1977 [6], in which, immersed elastic fibers with the same fluid density are modeled as a set of equivalent body forces in the Navier-Stokes equations. Since its inception, the immersed boundary method has been extended to a variety of problems, including design of prosthetic cardiac valves (McQueen and Peskin, 1985 [10]), swimming motions of marine worms (Fauci and Peskin, 1988 [12]), wood pulp fiber dynamics (Stockie and Wetton, 1999 [26]), wave propagation in cochlea (Beyer, 1992 [24]), and biofilm processes (Fogelson *et al.*, 1996 [9]). Recently, alternative procedures such the immersed interface method (LeVeque and Li, 1997 [23]) and the level set method (Sethian, 1996 [25]) have also been proposed to eliminate the numerical problems introduced by large motions of the immersed boundary. Furthermore, the effects of the flexibility, geometry, and mass of the immersed structures are amply demonstrated through the works of many other researchers [1] [2] [5] [45].

Immersed methods overcome many numerical problems such as severe fluid mesh

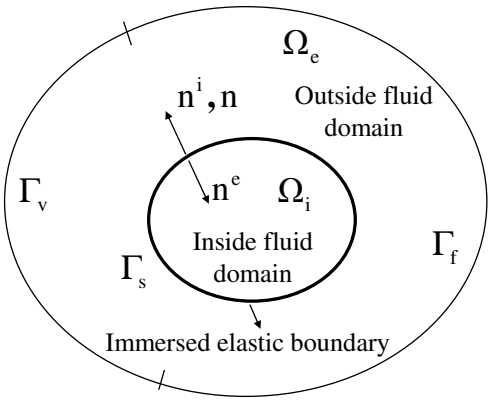

Figure 1: Immersed boundary illustration.

distortions encountered in traditional finite element methods (FEM) and computational fluid dynamics (CFD) procedures when modeling very flexible immersed structures [19] [27] [28] [31] [34]. With immersed methods, the issue of fluid mesh updates is resolved. However, in current immersed methods, complex structures/solids are still represented by elastic fiber networks. In the proposed immersed continuum method, sophisticated nonlinear finite element formulations will be introduced.

In Section 2, we recast the immersed boundary (IB) method (Peskin, 1977 [6]) into the traditional treatment of fluid-structure interactions by matching the kinematic and dynamic boundary conditions around the fluid-structure interface. In Section 3, we also show the theoretical foundations for some recent extensions of the immersed

boundary method using finite element formulations (Wang and Liu, 2004 [36], Zhang *et al.*, 2004 [44]). The new modeling procedure for immersed continua is presented to take into consideration of the compressibility of the submerged solid as well as the compressibility of the surround fluid. This formulation retains the same strategies as used in the immersed boundary method and its recently extensions, namely, the independent solid mesh moves on top of a fixed or even prescribed background fluid mesh.

3 Immersed Boundary Method Recast in FEM

In order to connect the immersed boundary method with the immersed continuum method using finite element formulations, we recast the immersed boundary method in the principle of virtual work, which to the author's best knowledge, is the first attempt. This recast not only demonstrates why the immersed boundary method works but also points to the linkage between the fictitious domain method and the proposed immersed continuum methods.

In Figs. 1 and 2, typical immersed boundary and immersed continuum systems are used to illustrate the difference between the current immersed methods which primarily handle immersed fibers and fiber networks and the proposed new methods which deal with arbitrary immersed structures/solids with finite volume and mass. The strong and weak forms which are the foundations for finite element procedures will be discussed based on the illustrations in Figs. 1 and 2. For simplicity, in this paper, we omit the superscript or subscript f for fluid variables.

Consider a fluid domain Ω enclosed with a sufficiently smooth boundary, $\partial\Omega = \Gamma_v \cup \Gamma_f$, where Γ_v and Γ_f stand for the Dirichlet and Neumann boundaries, respectively. Suppose there exists an enclosed boundary Γ_s (a line for two-dimensional cases and a

surface for three-dimensional cases) representing the immersed flexible boundary, the fluid domain Ω is separated into two regions, namely, the interior region Ω_i and the exterior region Ω_e. Therefore, the boundaries of the interior and the exterior regions can be simply expressed as $\partial\Omega_i = \Gamma_s$ and $\partial\Omega_e = \Gamma_s \cup \Gamma_v \cup \Gamma_f$. Denote $\boldsymbol{\sigma}$ as the stress tensor, $\mathbf{v}$ as the velocity vector, and ρ as the density in the fluid domain, the following governing equations (strong form) can be established:

$$\rho\dot{v}_i = \sigma_{ij,j} + f_i^{ext}, \text{ in } \Omega_i(\text{or } \Omega \setminus \Omega_e), \tag{3.1}$$

$$\rho\dot{v}_i = \sigma_{ij,j} + f_i^{ext}, \text{ in } \Omega_e, \tag{3.2}$$

$$[v_i] = 0, \text{ on } \Gamma_s, \text{ kinematic matching}, \tag{3.3}$$

$$[\sigma_{ij}n_j] = f_i^s + m\ddot{u}_i^s, \text{ on } \Gamma_s, \text{ dynamic matching}, \tag{3.4}$$

where in this paper, the external body forces f_i^{ext} are simply replaced by a typical example of gravitational forces ρg_i, with $\mathbf{g}$ as the gravitational acceleration; $\mathbf{f}^s$ and m stand for the elastic force and the mass density of the immersed boundary Γ_s (per unit length for two-dimensional cases and per unit area for three-dimensional cases); $\mathbf{u}^s$ denotes the interface displacement; and the surface normal vector $\mathbf{n}$ is aligned with that of the interior fluid domain $\mathbf{n}^i$ and opposite to that of the exterior fluid domain $\mathbf{n}^e$.

At this point, we can derive a number of numerical approaches to solving Eqs. (3.1) to (3.4). A straightforward approach is to represent the exterior and the interior fluid domains with different meshes and to match them accordingly at the interface Γ_s. This approach represents the traditional treatment of fluid-structure interaction problems, in which the solid mesh is coupled with the fluid mesh around the fluid-structure interface [19] [28].

Define the Sobolev space $[H^1_{0,\Gamma_v}(\Omega)]^d = \{\mathbf{w}| \quad \mathbf{w} \in [H^1(\Omega)]^d, \mathbf{w}|_{\Gamma_v} = \mathbf{0}\}$, where d represents the spatial dimensions, we express Eqs. (3.1) to (3.4) in the variational forms (weak form): $\forall \mathbf{w} \in [H^1_{0,\Gamma_v}(\Omega)]^d$

$$\int_{\Omega_i} w_i[\rho(\dot{v}_i - g_i) - \sigma_{ij,j}]d\Omega + \int_{\Omega_e} w_i[\rho(\dot{v}_i - g_i) - \sigma_{ij,j}]d\Omega = 0. \tag{3.5}$$

Notice that the immersed boundary Γ_s occupies no volume and yet separates the fluid domain Ω into the interior and exterior portions. The connection between these two fluid domains includes the continuity of the displacements through the kinematic matching and the balancing of the forces through the dynamic matching. Furthermore, using integration by parts and the divergence theorem, and combining the interior and exterior fluid domains with $\Omega_e \cup \Omega_i = \Omega$, Eq. (3.5) can be rewritten as: $\forall \mathbf{w} \in [H^1_{0,\Gamma_v}(\Omega)]^d$

$$\int_{\Omega} [w_i\rho(\dot{v}_i - g_i) + w_{i,j}\sigma_{ij}]d\Omega + \int_{\Gamma_s} w_i^s(f_i^s + m\ddot{u}_i^s)d\Gamma - \int_{\Gamma_f} w_i f_i^{\Gamma_f} d\Gamma = 0. \tag{3.6}$$

In the immersed boundary method, in particular for the explicit versions, we introduce the following two key equations:

$$f_i^{FSI} = -\int_{\Gamma_s} (f_i^s + m\ddot{u}_s)\delta(\mathbf{x} - \mathbf{x}^s)d\Gamma, \tag{3.7}$$

$$v_i^s = \int_{\Omega} v_i\delta(\mathbf{x} - \mathbf{x}^s)d\Omega, \tag{3.8}$$

where $\mathbf{f}^{FSI}$ is the so-called equivalent body force.

Note that Γ_s represents the current configuration of the submerged interface, and nonlinear mechanics is employed to relate the structural force $\mathbf{f}^s$ with the interfacial position $\mathbf{x}^s$ or the displacement $\mathbf{u}^s$. It is also clear that as long as we use the same delta function for both Eqs. (3.7) and (3.8), the virtual power input from the submerged flexible boundary (or the immersed boundary) to the fluid domain can be expressed as

$$\int_\Omega w_i f_i^{FSI} d\Omega = -\int_{\Gamma_s}\int_\Omega w_i \delta(\mathbf{x}-\mathbf{x}^s)(f_i^s + m\ddot{u}_i^s) d\Omega d\Gamma = -\int_{\Gamma_s} w_i^s (f_i^s + m\ddot{u}_i^s) d\Gamma. \quad (3.9)$$

Because Eq. (3.9) holds for all $\mathbf{w} \in [H^1_{0,\Gamma_v}(\Omega)]^d$, the effect of the submerged flexible boundary can be simply replaced with the equivalent body force $\mathbf{f}^{FSI}$. Hence the governing equations (3.1) to (3.4) can be rewritten as

$$\rho \dot{v}_i = \sigma_{ij,j} + \rho g_i + f_i^{FSI}, \text{ in } \Omega; \quad (3.10)$$

and the variational equations (3.5) and (3.6) are modified as

$$\int_\Omega [w_i(\rho \dot{v}_i - \rho g_i - f_i^{FSI}) + w_{i,j}\sigma_{ij}] d\Omega - \int_{\Gamma_f} w_i f_i^{\Gamma_f} d\Gamma = 0. \quad (3.11)$$

4 Fictitious Domain Approaches

Suppose there exists a rigid cylinder (for two-dimensional cases) or a rigid sphere (for three-dimensional cases) occupying a volume Ω_s in the total domain Ω. Again, around the fluid-solid interface Γ_s, the unit normal vector of the solid is $\mathbf{n}^s$ or $\mathbf{n}$ which points outward to the flow region and the unit normal vector of the fluid is denoted as $\mathbf{n}^f$ or $-\mathbf{n}$ which points inward to the submerged solid. Following the no-slip boundary condition on the interface Γ_s, we have

$$\mathbf{v}(\mathbf{x}, t) = \bar{\mathbf{v}}(t) + \bar{\boldsymbol{\omega}}(t) \times (\mathbf{x} - \bar{\mathbf{x}}(t)), \forall \mathbf{x} \in \Gamma_s, \quad (4.12)$$

where $\bar{\mathbf{x}}$, $\bar{\mathbf{v}}$, $\bar{\boldsymbol{\omega}}$, and $\mathbf{x}$ stand for the current position of the mass center, velocity, and angular velocity, and position on the interface of the rigid body.

Because the solid occupying Ω_s is a rigid body, Eq. (4.12) can be rewritten as

$$\mathbf{v}(\mathbf{x}^s, t) = \bar{\mathbf{v}}(t) + \bar{\boldsymbol{\omega}}(t) \times (\mathbf{x}^s - \bar{\mathbf{x}}(t)), \forall \mathbf{x}^s \in \Omega_s. \tag{4.13}$$

Of course, on the fluid-solid interface Γ_s, Eq. (4.13) is manifested as Eq. (4.12). Furthermore, the governing equations (strong form) of the fluid-solid system can be depicted as

$$\begin{aligned}
\rho_f \dot{v}_i &= \sigma_{ij,j} + \rho_f g_i, \text{ in } \Omega_f (\text{or } \Omega \setminus \Omega_s), && (4.14)\\
M\dot{\bar{v}}_i &= M g_i + F_i^s, \text{ for the rigid body } \Omega_s, && (4.15)\\
\mathbf{I}\dot{\bar{\boldsymbol{\omega}}} + \bar{\boldsymbol{\omega}} \times \mathbf{I}\bar{\boldsymbol{\omega}} &= \mathbf{T}^s, && (4.16)
\end{aligned}$$

where $\mathbf{I}$ and M are the rotational inertia tensor (or matrix) and the mass of the rigid body, respectively; and the resultant torque $\mathbf{T}^s$ and force $\mathbf{F}^s$ due to the fluid traction around the rigid body are expressed as

$$\begin{aligned}
\mathbf{T}^s &= -\int_{\Gamma_s} (\mathbf{x}^s - \bar{\mathbf{x}}) \times \boldsymbol{\sigma}\mathbf{n} d\Gamma, && (4.17)\\
\mathbf{F}^s &= -\int_{\Gamma_s} \boldsymbol{\sigma}\mathbf{n} d\Gamma. && (4.18)
\end{aligned}$$

In the fictitious domain method, an imaginary fluid is introduced to occupy the submerged solid domain Ω_s and to synchronize with the solid within Ω_s. With the fluid velocity variation $\mathbf{w} \in [H^1_{0,\Gamma_v}(\Omega)]^d$, the rigid body velocity variation $\bar{\mathbf{w}} \in R^d$, and the rigid body angular velocity variation $\bar{\boldsymbol{\theta}} \in R^d$, combining the solid domain with the fluid domain, employing integration by parts, the divergence theorem, and Eqs. (4.13), (4.17), and (4.18), we can convert the governing equations (strong form) in Eqs. (4.14) to (4.16) into the variational equations (weak form),

$$\int_{\Omega}[\rho w_i(\dot{v}_i - g_i) + w_{i,j}\sigma_{ij}]d\Omega + r[M(\dot{\bar{v}}_i - g_i)\bar{w}_i + (\mathbf{I}\dot{\bar{\boldsymbol{\omega}}} + \bar{\boldsymbol{\omega}} \times \mathbf{I}\bar{\boldsymbol{\omega}}) \cdot \bar{\boldsymbol{\theta}}] = 0, \tag{4.19}$$

with $r = 1 - \rho/\rho_s$.

The key treatment in the immersed boundary method and its extensions is to introduce the delta function to synchronize the fluid motion with the solid motion within the immersed structure/solid domain Ω_s, namely,

$$\mathbf{v}^s = \mathbf{v}^f. \tag{4.20}$$

In fact, the constraint of Eq. (4.20) introduces the (distributed) Lagrangian multiplier which acts as the equivalent body force. In the fictitious domain method, a similar (distributed) Lagrangian multiplier $\boldsymbol{\lambda}$ is introduced, along with the following traditional mixed formulation, we obtain, $\forall \mathbf{w} \in [H^1_{0,\Gamma_v}(\Omega)]^d$ and $\boldsymbol{\lambda} \in [H^1(\Omega_s)]^d$

$$\begin{aligned}&\int_{\Omega}[\rho_f w_i(\dot{v}_i - g_i) + w_{i,j}\sigma_{ij}]d\Omega + r[M(\dot{\bar{v}}_i - g_i)\bar{w}_i + (\mathbf{I}\dot{\bar{\boldsymbol{\omega}}} + \bar{\boldsymbol{\omega}} \times \mathbf{I}\bar{\boldsymbol{\omega}}) \cdot \bar{\boldsymbol{\theta}}] \\ &-(\boldsymbol{\lambda}, \mathbf{w} - \bar{\mathbf{w}} - \bar{\boldsymbol{\theta}} \times (\mathbf{x}^s - \bar{\mathbf{x}})) = 0,\end{aligned} \tag{4.21}$$

and

$$(\boldsymbol{\mu}, \mathbf{v} - \bar{\mathbf{v}} - \bar{\boldsymbol{\omega}} \times (\mathbf{x}^s - \bar{\mathbf{x}})) = 0, \forall \boldsymbol{\mu} \in [H^1(\Omega_s)]^d, \tag{4.22}$$

where the inner product is defined as

$$(\boldsymbol{\mu}, \boldsymbol{\lambda}) = \int_{\Omega_s}(\mu_i\lambda_i + l^2\mu_{i,j}\lambda_{i,j})d\Omega, \tag{4.23}$$

with a scaling factor l dependent of the characteristic length of Ω_s.

A clear advantage of the fictitious domain method is the use of the implicit formulation which does not involve the derivative of the delta function [13]. Nevertheless,

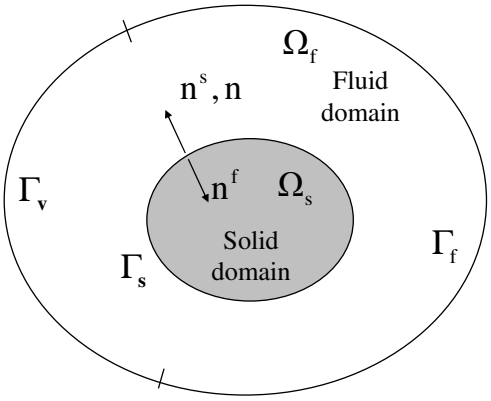

Figure 2: Immersed continuum illustration.

currently, such a formulation is limited to immersed rigid bodies. Since any rigid body is an incompressible body, the direct link between the fictitious incompressible fluid domain can be established. In addition, for incompressible viscous fluids, velocity/pressure formulation must also be used along with the distributed Lagrangian multiplier. A wealth of theoretical studies on the inf-sup conditions in particular those for three-field mixed finite element formulations are available in the context of the treatment of incompressible solids and fluids [3].

5 Immersed Continuum Method Formulation

Consider a fluid-solid system as illustrated in Fig. 2, the immersed deformable object occupies the time dependent domain $\Omega_s(t)$. As the solid domain $\Omega_s(t)$ evolves with time, the fluid domain $\Omega_f(t)$ or $\Omega \setminus \Omega_s(t)$ evolves as well. To circumvent this difficulty of variable fluid domains, we adopt the concept of the fictitious domain by introducing a deformable artificial fluid domain occupying the same domain for immersed solids $\Omega_s(t)$. As illustrated in Fig. 3, as long as we can enforce the fictitious fluid domain $\Omega_s(t)$ to match the immersed solid geometrically and in the mean time providing to the surrounding fluid the same virtual power input as the actual immersed solid, the original fluid-solid system can be replaced with a new fluid-solid system, in which the fluid domain is represented with an entire domain Ω and the immersed solid is represented with an initial solid subtracting the fictitious fluid occupying the same position $\Omega_s(t)$.

In this paper, we present the velocity/pressure formulation for the slightly compressible viscous fluid and the displacement/pressure formulation for the almost incompressible solid with a hyperelastic material model. This slight compressibility is crucial in the new formulation. In general, the immersed solid will be compressible, namely the total volume of the solid domain $\Omega(t)$ is also a function of time, therefore, the volume of the fictitious domain $\Omega(t)$ is also time-dependent. The kinematic matching condition requires a slight compressibility from the surrounding fluid. Of course, with the same deformations, the pressure introduced in the fictitious domain due to the fluid compressibility is different from that of the solid compressibility.

For stationary fluid domain Ω, we adopt an Eulerian kinematic description, therefore, the material derivative of the fluid velocity is expressed as

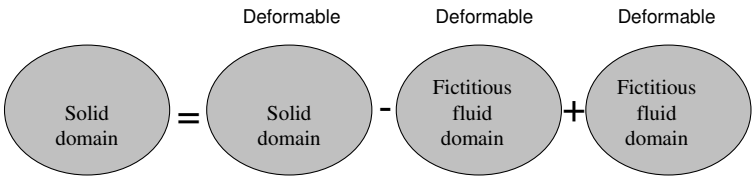

Figure 3: The adoption of the concepts of the fictitious domain method in the proposed immersed continuum method.

$$\dot{v}_i = v_{i,t} + v_j v_{i,j}. \tag{5.24}$$

Although we refer to the fixed background fluid mesh in the presentation of this paper, we must keep in mind that the Arbitrary Lagrangian-Eulerian (ALE) kinematic description [11] [34] can also be employed for time dependent fluid domain $\Omega(t)$ and the convective velocity in Eq. (5.24) must be replaced with $\mathbf{v} - \mathbf{v}^m$, where $\mathbf{v}^m$ stands for the given mesh velocity which governs the evolution of the entire fluid domain $\Omega(t)$. More elaborated discussion on this issue will be presented in a different paper by the author [35].

Adhere to the tradition, for convenience, we employ a Lagrangian kinematic description for the solid domain, thus the fluid-solid interface will be tracked automatically by the position of solid particles. Moreover, there is no need for convective terms in the solid domain and the material derivative is the same as the time derivative. Hence, the solid velocity vector $\mathbf{v}^s$ and the acceleration vector $\dot{\mathbf{v}}^s$ can be expressed as

$$\mathbf{v}^s = \dot{\mathbf{u}}^s \text{ and } \dot{\mathbf{v}}^s = \ddot{\mathbf{u}}^s, \tag{5.25}$$

with the displacement vector $\mathbf{u}^s(t) = \mathbf{x}^s(t) - \mathbf{x}^s(0)$, where $\mathbf{x}^s(t)$ and $\mathbf{x}^s(0)$ stand for the current and the original material point positions within the solid domain Ω_s.

We must also point out that the solid domain Ω_s and the material point position $\mathbf{x}^s$ all refer to the current solid configurations, and therefore for clarity could be denoted as $\Omega_s(t)$ and $\mathbf{x}^s(t)$, respectively.

In order to deal with the compressible viscous fluid, we subtract the pressure p from the stress components σ_{ij} to obtain the deviatoric stress components τ_{ij}, which is illustrated in a Newtonian fluid model as

$$\sigma_{ij} = -p\delta_{ij} + \tau_{ij}, \tag{5.26}$$

with $\tau_{ij} = 2\mu(e_{ij} - e_{kk}/3\delta_{ij})$ and $e_{ij} = (v_{j,i} + v_{i,j})/2$.

Furthermore, to couple with the unknown pressure, the continuity equation of the compressible viscous fluid is expressed as

$$v_{i,i} + \frac{\dot{p}}{\kappa} = 0, \tag{5.27}$$

where κ is the bulk modulus of the fluid; and the material derivative $\dot{p}$ can be simply expressed as $p_{,t} + v_i p_{,i}$ or $p_{,t} + (v_i - v_i^m)p_{,i}$ for the Eulerian or Arbitrary Lagrangian-Eulerian descriptions, respectively.

In the analysis of slightly compressible fluids, we assume the compressibility measured by bulk modulus κ is constant. Therefore, we have the following relationship between the density and the pressure of the fluid domain,

$$\frac{dp}{d\rho} = c^2 = \frac{\kappa}{\rho}. \tag{5.28}$$

From Eq. (5.28), it is straightforward to derive the following

$$p(t) - p(0) = \kappa \ln \frac{\rho(t)}{\rho(0)}. \tag{5.29}$$

Like the fluid stress tensor, we also decompose the solid stress tensor as a hydrostatic pressure p^s, and a deviatoric stress tensor τ_{ij}^s,

$$\sigma_{ij}^s = -p^s\delta_{ij} + \tau_{ij}^s. \tag{5.30}$$

Unlike the fluid domain, since we use the Lagrangian description for the submerged solid, the treatments of the continuity equation and the Cauchy stress in nonlinear

solid mechanics are not as straightforward. As a special case, if the submerged solid is a flexible structure with a linear elastic material law, we will only have the geometrical nonlinearity to deal with. In this case, suppose the Young's modulus and the Poisson ratio are E and ν, respectively, and the bulk modulus for the solid can be simply expressed as $\kappa^s = E/3(1-2\nu)$. However, Cauchy stress must still be depicted on the current configuration which itself is unknown.

In this work, we discuss a nonlinear solid mechanics model with both the geometrical and material nonlinearities [36] [44]. First of all, we must introduce the solid deformation gradient $F_{ij} = \partial x_i^s(t)/\partial x_j^s(0)$, from which we can derive the Green-Lagrangian strain ϵ_{ij}. To obtain the energy conjugate stress S_{ij}, the second Piola-Kirchhoff stress, we must first introduce the elastic energy $\bar{W}$, which is often related to the three invariants of the Cauchy-Green deformation tensor $\mathbf{C}$ defined as $\mathbf{F}^T\mathbf{F}$. Moreover, as discussed in Refs. [15] and [38], an elastic energy term $-[p^s + \kappa^s(J_3 - 1)]^2/2\kappa^s$ is added to $\bar{W}$, along with the solid unknown pressure p^s introduced as

$$J_3 - 1 + \frac{p^s}{\kappa^s} = 0, \tag{5.31}$$

where κ^s is the solid bulk modulus and J_3 stands for the determinant of the deformation gradient.

Of course, to match with the expression in Eq. (5.30), the solid Cauchy stress is converted from the second Piola-Kirchhoff stress,

$$\sigma_{ij}^s = \frac{1}{\det(\mathbf{F})} F_{i,m} S_{mn} F_{j,n}. \tag{5.32}$$

Finally, since the solid displacement is dependent on the fluid velocity, the primary unknowns for the coupled fluid-solid system are the fluid velocity $\mathbf{v}$, the fluid pressure p, and the solid pressure p^s.

Define the Sobolev spaces, so the weak form of governing equations can be modified as: $\forall q \in L^2(\Omega)$, $q^s \in L^2(\Omega_s)$, $\mathbf{w} \in [H^1_{0,\Gamma_v}(\Omega)]^d$, which includes $\forall \mathbf{w}^s \in [H^1(\Omega_s)]^d$, and find $\mathbf{v}$ and p in Ω, p^s in Ω_s, such that

$$\begin{aligned}
&\int_\Omega w_i \rho(\dot{v}_i - g_i) d\Omega + \int_\Omega (w_{i,j}\tau_{ij} - p w_{i,i}) d\Omega - \int_{\Gamma_f} w_i f_i^{\Gamma_f} d\Gamma \\
&+ \int_{\Omega_s} [w_i^s(\rho_s - \rho)(\dot{v}_i - g_i) + w^s_{i,j}(\tau^s_{ij} - \tau^f_{ij}) - (p^s - p) w^s_{i,i}] d\Omega + \\
&+ \int_\Omega q(v_{j,j} + \frac{p_{,t}}{\kappa}) d\Omega + \int_{\Omega_s} q^s (J_3 - 1 + \frac{p^s}{\kappa^s}) d\Omega = 0.
\end{aligned} \tag{5.33}$$

Note that within the domain Ω_s the fluid deviatoric stress τ^f_{ij} is calculated with the fluid formulations. Using integration by parts and the divergence theorem, we establish the following strong form:

$$\rho_s \dot{v}^s_i = -p^s_{,i} + \tau^s_{ij,j} + \rho_s g_i, \text{ in } \Omega_s (\text{or } \Omega \setminus \Omega_f), \tag{5.34}$$

$$p^s = -\kappa^s (J_3 - 1), \text{ in } \Omega_s, \tag{5.35}$$

$$\rho \dot{v}_i = -p_{,i} + \tau_{ij,j} + \rho g_i, \text{ in } \Omega_f, \tag{5.36}$$

$$p_{,t} = -\kappa v_{j,j}, \text{ in } \Omega_f, \tag{5.37}$$

$$[v_i] = 0, \text{ on } \Gamma_s, \text{ kinematic matching}, \tag{5.38}$$

$$[\sigma_{ij} n_j] = 0, \text{ on } \Gamma_s, \text{ dynamic matching}, \tag{5.39}$$

where the surface normal vector $\mathbf{n}$ is aligned with that of the solid domain $\mathbf{n}^s$ and is opposite to that of the fluid domain $\mathbf{n}^f$.

We recognize that there are two sets of discretizations, namely, one for the Lagrangian solid mesh and the other one for the Eulerian fluid mesh. In this paper, the discretization of the fluid domain is identical to the stabilized Galerkin formulation for the Navier-Stokes equations [27] [28] [30]. It is clear that different numerical schemes

for fluid flows such as the flow-condition-based interpolation finite element scheme [4] or the lattice Boltzmann method [42] can also be employed in the immersed continuum method as the fluid solver.

In this paper, we introduce for the fluid domain the following interpolations for the entire domain Ω:

$$\mathbf{v}^h = N_I^v \mathbf{v}_I, \quad \mathbf{w}^h = N_I^v \mathbf{w}_I, \quad p^h = N_I^p p_I, \quad q^h = N_I^p q_I, \tag{5.40}$$

where N_I^v and N_I^p stand for the interpolation functions at node I for the velocity vector and the pressure; and $\mathbf{v}_I$, $\mathbf{w}_I$, p_I, and q_I are the nodal values of the discretized velocity vector, admissible velocity variation, pressure, and pressure variation, respectively.

Notice that in general the interpolation functions for the velocity vector and the unknown pressures are different. Therefore, we retain the superscripts v and p to denote such differences. Furthermore, we ignore the change of the fluid density due to the pressure change.

Likewise for the solid domain Ω_s, the discretization is based on the following:

$$\mathbf{u}^{s,h} = N_J^u \mathbf{u}_J^s, \quad \mathbf{w}^{s,h} = N_J^u \mathbf{w}_J^s, \quad p^{s,h} = N_J^{p^s} p_J^s, \quad q^{s,h} = N_J^{p^s} q_J^s, \tag{5.41}$$

where N_J^u and $N_J^{p^s}$ stand for the interpolation functions at node J for the displacement vector and the unknown pressures; and $\mathbf{u}_J^{s,h}$, $\mathbf{w}_J^{s,h}$, $p_J^{s,h}$, and $q_J^{s,h}$ are the nodal values of the discretized displacement vector, admissible velocity variation, pressure, and pressure variation, respectively.

Substituting both discretizations (5.40) and (5.41) into Eq. (5.33), we obtain the following discretization of the weak form: $\forall q^h \in L^2(\Omega^h)$, $q^{s,h} \in L^2(\Omega_s^h)$, $\mathbf{w}^h \in [H^{1,h}_{0,\Gamma_v^h}(\Omega^h)]^d$, which includes $\forall \mathbf{w}^{s,h} \in [H^{1,h}(\Omega_s^h)]^d$,

$$\int_{\Omega^h} w_{iI} N_I^v \rho \dot{v}_i^h d\Omega - \int_{\Gamma_f^h} w_{iI} N_I^v f_i^{\Gamma_f^h} d\Gamma + \int_{\Omega^h} (w_{iI} N_{I,j}^v \tau_{ij} - p^h w_{iI} N_{I,i}^v) d\Omega$$
$$+ \int_{\Omega_s^h} [w_{iJ}^s N_J^u (\rho_s - \rho)(\dot{v}_i^h - g_i) + w_{iJ}^s N_{J,j}^u (\sigma_{ij}^s - \sigma_{ij}^f)] d\Omega - \int_{\Omega^h} w_{iI} N_I^v \rho g_i d\Omega \qquad (5.42)$$
$$+ \int_{\Omega^h} q_I N_I^p (v_{j,j}^h + \frac{p_{,t}^h}{\kappa}) d\Omega + \int_{\Omega_s^h} q_J^s N_J^{p^s} (J_3 - 1 + \frac{p^{s,h}}{\kappa^s}) d\Omega = 0.$$

The key of the immersed continuum method is to recognize the fact that the non-linear mapping from $\mathbf{w}_I$ to $\mathbf{w}_J^s$, namely, from the fluid mesh to the solid mesh is derived from the discretized constraint of the velocities of the immersed solid and the corresponding fluid occupying the same solid domain. It turns out that such discretized mapping using various kernel functions has been studied recently in the meshless finite element methods. For example, the reproducing kernel particle method (RKPM) was proposed as an alternative or enhancement to various numerical procedures including finite element methods (Liu *et al.*, 1995 and 1996, [39] [40] [41] and Li and Liu, 1999 [21]). Unlike the discretized delta function in the immersed boundary method [7], the kernel functions in the meshless methods can handle non-uniform meshing, which marks an important improvement for the increase of the local resolutions near the interfaces. Furthermore, the adjustable reproducing properties of the meshless kernels enable a better representation of the discretized delta function in the frequency domain, namely, as the polynomial order $n \to \infty$, the discretized delta function ϕ becomes flatter at $\omega = 0$ and approaches to an ideal filter in the frequency domain. A detailed discussion of the delta function can be found in Refs. [36] [44].

Hence, at a typical solid node J, with a finite support domain Ω_J, the discretized form of the constraint of the velocities of the immersed solid and the corresponding fluid occupying the same solid domain can be expressed as

$$\mathbf{v}_J^s = \sum_I \mathbf{v}_I \phi_I(\mathbf{x}_I - \mathbf{x}_J^s) \text{ and } \mathbf{w}_J^s = \sum_I \mathbf{w}_I \phi_I(\mathbf{x}_I - \mathbf{x}_J^s), \forall \mathbf{x}_I \in \Omega_J, \tag{5.43}$$

where $\phi_I(\mathbf{x}_I - \mathbf{x}_J)$ is the kernel function centered at the solid node J, represented with $\mathbf{x}_J^s$.

It is very important to realize that the material points of the submerged solid domain will move in the entire domain, therefore even if we do not adjust the size of the support domain attached to these material points, Eq. (5.43) represents a nonlinear mapping which in this work for convenience is simply denoted as $\tilde{N}$.

Note that in general within the solid domain, we can ignore the stress components computed using the fluid model. If however we want to include the stress difference $\sigma_{ij}^s - \sigma_{ij}^f$ or $-(p^s - p^f)\delta_{ij} + (\tau_{ij}^s - \tau_{ij}^f)$ within the solid mesh, in addition to the mapping of the velocity vector in Eq. (5.43). In order to use the definition of σ_{ij}^f, we must also map the unknown pressure from the fluid mesh denoted with node I to the solid mesh denoted with node J. Therefore, like Eq. (5.43), we have

$$p_J^f = \sum_I p_I \phi_I(\mathbf{x}_I - \mathbf{x}_J), \forall \mathbf{x}_I \in \Omega_J. \tag{5.44}$$

Finally for the entire domain Ω, due to the arbitrariness of the variations w_{iI}, q_I, and q_J^s, we have four equations at each fluid node I and one equation at each solid node J,

$$r_{iI}^v = 0, \quad r_I^p = 0, \quad r_J^{p^s} = 0, \tag{5.45}$$

where the residuals are defined as

$$
\begin{aligned}
r^v_{iI} &= \int_{\Omega^h} N^v_I \rho \dot{v}^h_i d\Omega + \int_{\Omega^h} [N^v_{I,j}\tau_{ij} - p^h N^v_{I,i}] d\Omega - \int_{\Gamma^h_f} N_I^{v,\Gamma^h_f} f_i^{\Gamma^h_f} d\Gamma \\
&\quad + \int_{\Omega^h_s} \tilde{N}[N^u_J(\rho_s - \rho)(\dot{v}^h_i - g_i) + N^u_{J,j}(\sigma^s_{ij} - \sigma^f_{ij})] d\Omega - \int_{\Omega^h} N^v_I \rho g_i d\Omega, \\
r^p_I &= \int_{\Omega^h} N^p_I (v^h_{j,j} + \frac{p^h_{,t}}{\kappa}) d\Omega, \\
r^{p^s}_J &= \int_{\Omega^h_s} N^{p^s}_J (J_3 - 1 + \frac{p^{s,h}}{\kappa^s}) d\Omega.
\end{aligned}
\tag{5.46}
$$

Note that the convective terms are hidden in $\dot{v}^h_i$ and the detailed expressions of the stabilized Galerkin formulation for the Navier-Stokes equations are identical to those employed in the stabilized Galerkin formulations [27] [28] [30] [44].

For clarity, we introduce a displacement nodal unknown vector $\mathbf{U}$, although it is only evaluated in the solid domain Ω_s in which a Lagrangian description is prescribed. In fact, within the solid domain, $\mathbf{U}$ is denoted as $\mathbf{U}^s$ and evolves based on $\mathbf{V}^s$ and $\dot{\mathbf{V}}^s$ which are mapped from the velocity nodal unknown vector $\mathbf{V}$ and acceleration nodal unknown vectors $\dot{\mathbf{V}}$ for the fluid domain. Mathematically, we could say that $\mathbf{v}^s$ is $\mathbf{v}$ directly evaluated at the material point $\mathbf{x}^s$. Likewise, the pressure nodal unknown vectors $\mathbf{P}$ and $\mathbf{P}^s$ are introduced for the fluid and solid domains, respectively. Moreover, in the discussion of numerical procedures, we denote the time derivative of a variable a as $\dot{a}$. In this paper, for simplicity, we adopt a form of Newton-Raphson iteration, and apply the Newmark time integration scheme as discussed in Refs. [15] [16] [29] [32] [33]. For a typical state variable a, in the incremental analysis, we have

$$
\begin{aligned}
a(t+\Delta t) &= a(t) + \dot{a}(t)\Delta t + [(0.5-\alpha)\ddot{a}(t) + \alpha \ddot{a}(t+\Delta t)]\Delta t^2, \\
\dot{a}(t+\Delta t) &= \dot{a}(t) + [(1-\beta)\ddot{a}(t) + \beta \ddot{a}(t+\Delta t)]\Delta t,
\end{aligned}
\tag{5.47}
$$

where the unknown a stands for the scaler components of the nodal or discretized variables for $\mathbf{V}$, $\mathbf{P}^s$, and $\mathbf{P}$, and α and β are selected integration constants.

As a consequence, at every time step, the nonlinear residual equations (5.46) can be simply written as

$$\mathbf{r}(\mathbf{V}, \mathbf{P}, \dot{\mathbf{V}}, \dot{\mathbf{P}}, \mathbf{P}^s) = \mathbf{0}. \tag{5.48}$$

6 Matrix-Free Newton-Krylov Iteration

6.1 Basic Concepts

In the k^{th} Newton-Raphson iteration at time step $m+1$ of the nonlinear residual equation (5.48), from $\mathcal{R}^N$ to $\mathcal{R}^N$, with N as the number of the total unknowns, we start with a first guess of the incremental unknowns $\Delta\mathbf{\Theta}^{k,0}$, namely, $\Delta\mathbf{V}^0$, $\Delta\mathbf{P}^0$, and $\Delta\mathbf{P}^{s,0}$, which often are zero vectors. Then the residual of the linearized systems of equations at the k^{th} Newton-Raphson iteration is evaluated as

$$\mathbf{p} \;=\; -\mathbf{r}^{m+1,k-1} - \mathbf{r}_{,v}^{m+1,k-1}\Delta\mathbf{V}^0 - \mathbf{r}_{,p}^{m+1,k-1}\Delta\mathbf{P}^0 - \mathbf{r}_{,p^s}^{m+1,k-1}\Delta\mathbf{P}^{s,0}. \tag{6.49}$$

This error vector is used to construct the n-dimensional Krylov subspace $\mathcal{K}^n = span\{\mathbf{p}, \mathbf{J}\mathbf{p}, \mathbf{J}^2\mathbf{p}, \ldots, \mathbf{J}^{n-1}\mathbf{p}\}$ where $\mathbf{J}$ is the $N \times N$ Jacobian matrix evaluated at time step $m+1$ and the k^{th} Newton-Raphson iteration of the nonlinear residual equation (5.48) and can be rewritten as

$$\mathbf{J} = (\mathbf{r}_{,v}^{m+1,k-1}, \mathbf{r}_{,p}^{m+1,k-1}, \mathbf{r}_{,p^s}^{m+1,k-1}). \tag{6.50}$$

The approximate solution $\Delta\mathbf{\Theta}$ is written as the combination of the initial guess $\Delta\mathbf{\Theta}^{k,0}$ and $\mathbf{z}^n$, with $\mathbf{z}^n \in \mathcal{K}^n$. Note that the dimension of the subspace $\mathcal{K}^n$ is n which is much smaller than the dimension N of the unknown vector $\Delta\mathbf{\Theta}$. The N-dimensional unknown vector $\Delta\mathbf{\Theta}$ or rather $\mathbf{z}^n$ is represented with $\mathbf{V}_n\mathbf{y}$, where $\mathbf{y}$ is a

much smaller n-dimensional unknown vector. In the Generalized Minimum Residual (GMRES) method, the modified Gram-Schmidt orthogonalization procedures are used to derive a set of orthonormal vectors v_i, with $1 \leq i \leq n$ in the Krylov space $\mathcal{K}^n$ and an $(n+1) \times n$ upper-Hessenberg matrix $\bar{\mathbf{H}}_n$. Define $\mathbf{V}_n = (\mathbf{v}_1 \mathbf{v}_2 \dots \mathbf{v}_n)$ and $\mathbf{V}_{n+1} = (\mathbf{v}_1 \mathbf{v}_2 \dots \mathbf{v}_{n+1})$, we have the following

$$\mathbf{J}\mathbf{V}_n = \mathbf{V}_{n+1}\bar{\mathbf{H}}_n. \tag{6.51}$$

The remaining process in the GMRES method is to solve the least square problem

$$\min_{\mathbf{z}\in\mathcal{K}^n} \|\mathbf{p} - \mathbf{J}\mathbf{z}\| \text{ or } \min_{\mathbf{y}\in\mathcal{R}^n} \|\mathbf{p} - \mathbf{J}\mathbf{V}_n\mathbf{y}\|. \tag{6.52}$$

Assume γ is the length of the initial residual vector $\mathbf{p}$ and $\mathbf{e}_1$ is the unit vector representing the first column of $(n+1)\times(n+1)$ identity matrix, substituting Eq. (6.51), we can show that Eq. (6.52) is equivalent to the following minimization within a much smaller space

$$\min_{\mathbf{y}\in\mathcal{R}^n} \|\gamma\mathbf{e}_1 - \bar{\mathbf{H}}_n\mathbf{y}\|, \tag{6.53}$$

6.2 Preconditioning and Algorithm

In the matrix-free Newton-Krylov iteration, we do not form the Jacobian matrix. In general, this Jacobian matrix in the immersed boundary/continuum methods has an $O(n^2)$ storage requirement. For large systems with million degrees of freedoms, this Jacobian matrix requires a terabyte (10^{12}) memory which is beyond the limit of computational facilitates available for most scientific researches. It is based on this understanding, we would also like to design a preconditioning technique without the use of the Jacobian matrix [8] [14] [22].

First of all, the initial residual vector $\mathbf{p}$ in the k^{th} Newton-Raphson iteration at time step $m+1$ of the nonlinear residual equation (5.48) is normalized as $\mathbf{v}_1$ with the length $\gamma = \|\mathbf{p}\|_2$. Using Eq. (6.53), we have the corresponding n dimensional residual vector $\mathbf{b} = \gamma \mathbf{e}_1$. Introduce a preconditioning matrix $\mathbf{\Lambda}$, for $i = 1$ to n, using the modified Gram-Schmidt orthogonalization process, we have $\mathbf{q}_i = \mathbf{\Lambda}^{-1}\mathbf{v}_i$ and $\mathbf{w} = \mathbf{J}\mathbf{q}_i$, and for $j = 1$ to i, we have $h_{ji} = \mathbf{w}^T\mathbf{v}_j$ and $\mathbf{w}$ is updated with $\mathbf{w} - h_{ji}\mathbf{v}_j$. As a consequence, we obtain $h_{(i+1)i} = \|\mathbf{w}\|_2$ and $\mathbf{v}_{i+1} = \mathbf{w}/h_{(i+1)i}$.

An important procedure in the matrix-free Newton-Krylov is to replace $\mathbf{w} = \mathbf{J}\mathbf{q}_i$ with a finite difference based calculation,

$$\mathbf{J}\mathbf{q}_i \simeq \frac{\mathbf{r}(\mathbf{\Theta}^{m+1,k-1} + e\mathbf{q}_i) - \mathbf{r}(\mathbf{\Theta}^{m+1,k-1})}{e}, \tag{6.54}$$

where e is often set to be around the square root of the machine error [8].

After we establish the elements of an upper $n \times n$ Hessenberg matrix $\mathbf{H}_n$ as well as an upper $(n+1) \times n$ Hessenberg matrix $\bar{\mathbf{H}}_n$, for $j = 1$ to n, and $i = 1$ to $j-1$, a factorization of $\mathbf{H}_n$ is carried out through the following rotation matrix operations,

$$\begin{array}{rcl} h_{ij} & = & c_i h_{ij} + s_i h_{(i+1)j}, \\ h_{(i+1)j} & = & -s_i h_{ij} + c_i h_{(i+1)j}, \end{array} \tag{6.55}$$

where the entities of the rotation processes are calculated as

$$r = \sqrt{h_{jj}^2 + h_{(j+1)j}^2}, \quad c_j = h_{jj}/r, \text{ and } s_j = h_{(j+1)j}/r. \tag{6.56}$$

Through this rotation process, the upper Hessenberg matrix is converted to a diagonal matrix with the coefficients defined as: for $j = 1$ to n

$$h_{jj} = r, \quad p_j = c_j b_j, \text{ and } p_{j+1} = -s_j b_j. \tag{6.57}$$

Finally, the termination criteria of the GMRES iteration will rest at the absolute value of b_{n+1} in comparison with a given error ϵ. If $|b_{n+1}| < \epsilon$, the solution vector $\Delta\mathbf{\Theta}$, or rather $\Delta\mathbf{V}$, $\Delta\mathbf{P}$, and $\Delta\mathbf{P}^s$ is expressed as

$$\Delta\mathbf{\Theta}^{k,n} = \Delta\mathbf{\Theta}^{k,0} + \sum_{i=1}^{n} y_i \mathbf{q}^i, \text{ or } \begin{bmatrix} \Delta\mathbf{V} \\ \Delta\mathbf{P} \\ \Delta\mathbf{P}^s \end{bmatrix} = \Delta\mathbf{\Theta}^{k,0} + \sum_{i=1}^{n} y_i \mathbf{q}^i. \tag{6.58}$$

As a final remark, if the initial guess $\Delta\mathbf{\Theta}^{k,0}$ does not produce a good estimate within a sufficiently small Krylov subspace $\mathcal{K}^n$. $\Delta\mathbf{\Theta}^{k,n}$ will be introduced as an updated initial guess and the GMRES iteration procedure will continue until a solution with the desired accuracy is obtained.

7 Numerical Examples

REVISED A program based on the flow chart in Fig 4 is used to test the proposed numerical procedures. Although rigorous studies of this type of immersed methods are not yet available, we present a set of preliminary numerical examples. In the first example, a deformable cylinder or disk with a diameter of $2a$ is released in a viscous fluid channel. The physical parameters of this set of test cases are given as follows: acceleration due to gravitation $g = 9.81\ m/s^2$; dynamic viscosity $\mu = 1\ dyne/cm^2 \cdot s$; and fluid density $\rho_f = 1\ g/cm^3$. To implement the effect of gravity, an external body force is only applied to the cylinder. The buoyancy is captured by the definition of the mass matrix. In general, the flexibility of the cylinder decreases the surrounding fluid forces (viscous shear, form drag, etc.) and as a consequence increases the terminal velocity. In this example, the submerged solid is made of an almost incompressible rubber material with the material constants $C_1 = 29300$, $C_2 = 17700$, and $\kappa = 141000\ dyne/cm^2$ and the

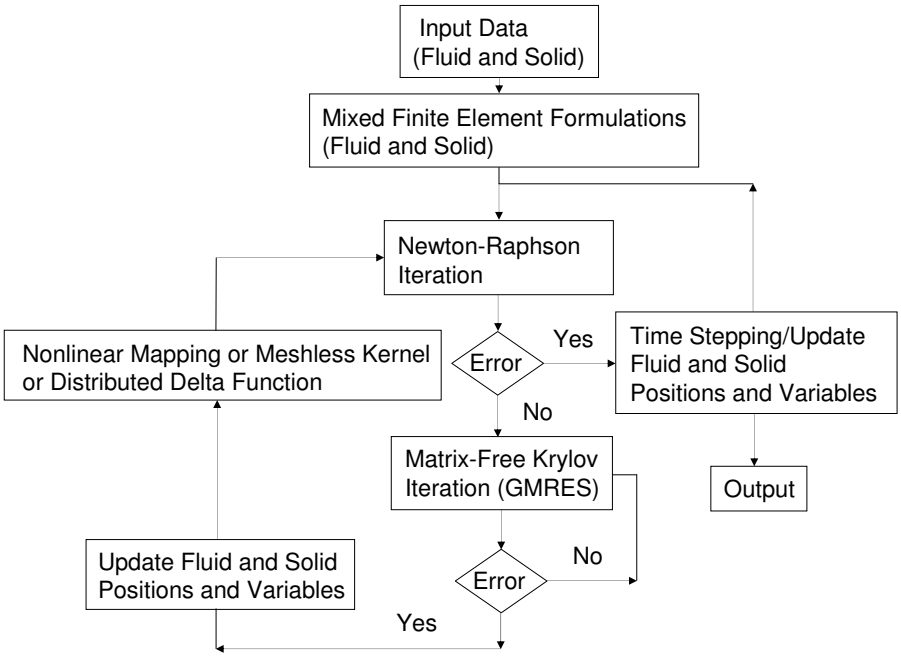

Figure 4: The adoption of the concepts of the fictitious domain method in the proposed immersed continuum method.

density $\rho_s = 3\ g/cm^3$.

In Fig. 5, it is shown that for a very flexible object ($C_1 = 2.93$, $C_2 = 1.77$, and $\kappa = 1.41\ dyne/cm^2$) moving in a highly viscous environment ($\mu = 10\ dyne/cm^2 \cdot s$), the proposed numerical procedure can be used to capture both the normal and shear stress distributions within the moving solid domain and the results are comparable with those derived from the extended immersed boundary method [36].

In another example, a chain of three deformable objects with the similar material properties are released and move towards to an elastic bifurcation.

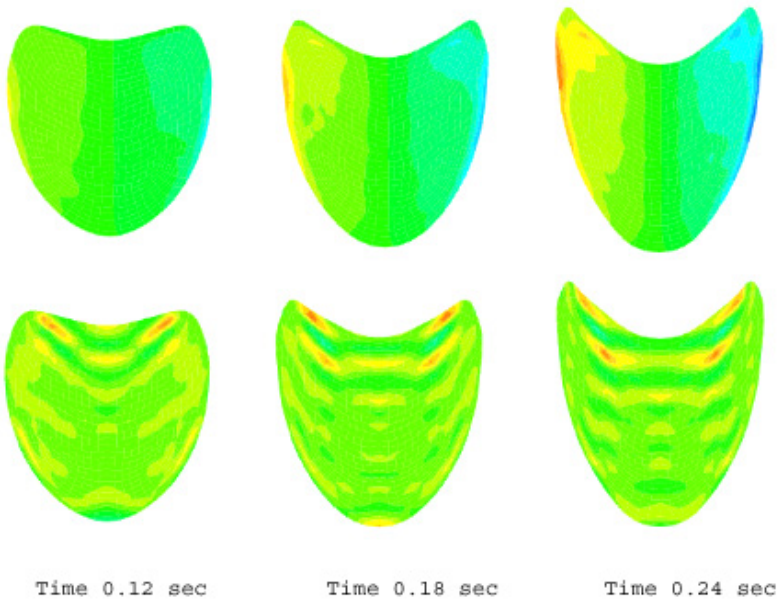

Figure 5: Shear and pressure bandplots of the deformable disk falling in a highly viscous fluid.

Initially, these objects are perfectly centered and aligned with the bifurcation point. What breaks the symmetry is the slight difference between the upper and lower branches of the bifurcation. As shown in Fig. 6, objects impact, deform, and conform with the viscous flow within the lower branch of the bifurcation. This type of study is very important for the understanding of the adverse effects of artificial devices exerted on red blood cells.

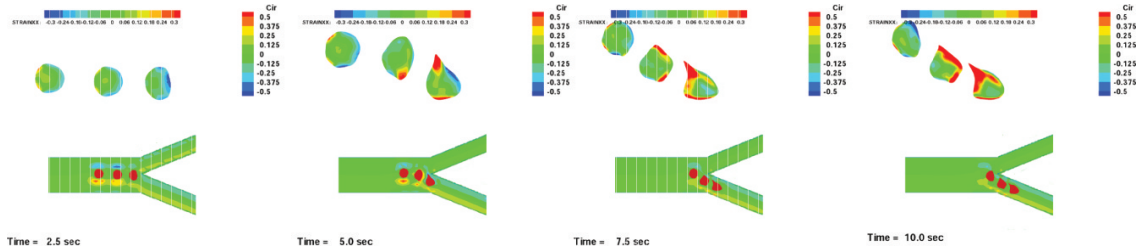

Figure 6: Three deformable objects impact the elastic bifurcation point and conform to the flow within the lower branch.

A typical fluid-structure interaction system is solved with two approaches, namely, the Newton-Raphson iteration with a direct solver and the matrix-free Netwon-Krylov iteration with a preconditioner. It is confirmed that both approaches yield the same results. A detailed digit by digit comparison also confirms that the velocity and pressure results differ only after the 5 or 6 decimal points which is consistent with the error criteria set for the Netwon-Krylov iteration.

To quantify the effectiveness of the preconditioner, we compare a typical fluid-structure interaction problem using the matrix-free Newton-Krylov iteration procedures with and without the preconditioner. The total number of time steps is 40. Three criteria are used, namely, the number of Newton-Raphson iterations per time step, the number of GMRES iterations per

20 Time Steps Step Size 0.07 s	Preconditioner With	Preconditioner Without
Newton Iterations	5	12
GMRES Iterations	2	10
CPU Time (s)	2168	10721

Table 1: Comparison of the matrix-free Newton-Krylov iterative procedures.

Newton-Raphson iteration, and the total CPU time in seconds. As demonstrated in Tab. 1, it is evident that the preconditioner is very effective in all three categories. Notice that with the preconditioner the maximum number of GMRES iteration stays at two for all time steps and Newton-Raphson iterations. Finally, the results of the solutions with and without the preconditioner are within the iterative error bounds, in this case, set to be as 10^{-5}, less than the square root of the machine roundoff error 10^{-15}.

8 Conclusion

The coupling of fluids and solids is the central feature in the study of the mechanics of the heart, arteries, veins, microcirculation, and pulmonary blood flow. Currently, the modelling of strong hemodynamic interaction with flexible structures is limited by severe fluid mesh distortions around flexible structures with large deformations and displacements. Recent breakthrough has been made in extending the concepts of the immersed boundary method to finite element formulations [36] [37] [44]. In the formulation presented in this paper, independent finite element meshes for immersed solids are introduced to couple with the finite element meshes for the background fluid. Both sets of meshes are non-uniform and the coupling is accomplished through kernel functions employed in meshless methods [39] [40] [41]. Rather than identify

and follow the fluid-structure interfaces in conventional approaches, we substitute the entire submerged solids with a collection of immersed Lagrangian nodal points, and as a consequence, automatically define the interfaces with the material points enclosing the solid domains. This method promises to provide an easy treatment of complex fluid-solid systems in particular those with immersed flexible solids and hence a platform or linkage for multi-scale and multi-physics modelling of biological systems.

9 Acknowledgment

The supports from NASA Langley and NSF (DMI-0503652 and BES-0503649) are greatly acknowledged.

References

[1] A.-K. Tornberg and M. Shelley. Simulating the dynamics and interactions of flexible fibers in stokes flows. *Journal of Computational Physics*, 196:8–40, 2004.

[2] S. Alben, M. Shelley, and J. Zhang. Drag reduction through self-similar bending of a flexible body. *Nature*, 420:479–481, 2002.

[3] W. Bao, X. Wang, and K.J. Bathe. On the Inf-Sup condition of mixed finite element formulations for acoustic fluids. *Mathematical Models & Methods in Applied Sciences*, 11:883–901, 2001.

[4] K.J. Bathe and H. Zhang. Finite element developments for general fluid flows with structural interactions. *International Journal for Numerical Methods in Engineering*, 60:213–232, 2004.

[5] C. Yang, D. Tang, and S.Q. Liu. A multi-physics growth model with fluid-structure interactions for blood flow and re-stenosis in rat vein grafts. *Computers & Structures*, 81:1041–1058, 2003.

[6] C.S. Peskin. Numerical analysis of blood flow in the heart. *Journal of Computational Physics*, 25:220–252, 1977.

[7] C.S. Peskin. The immersed boundary method. *Acta Numerica*, 11:479–517, 2002.

[8] D.A. Knoll and D.E. Keyes. Jacobian-free Newton-Krylov methods: a survey of approaches and applications. *Journal of Computational Physics*, 193:357–397, 2004.

[9] R. Dillon, L. Fauci, A. Fogelson, and D. Gaver III. Modeling biofilm processes using the immersed boundary method. *Journal of Computational Physics*, 129:57–73, 1996.

[10] D.M. McQueen and C.S. Peskin. Computer-assisted design of butterfly bileaflet valves for the mitral position. *Scand. J. Thor. Cardiovasc. Surg.*, 19:139–148, 1985.

[11] J. Donea, S. Giuliani, and J.P. Halleux. An arbitrary Lagrangian-Eulerian finite element method for transient dynamic fluid-structure interactions. *Computer Methods in Applied Mechanics and Engineering*, 33:689–723, 1982.

[12] L.J. Fauci and C.S. Peskin. A computational model of aquatic animal locomotion. *Journal of Computational Physics*, 77:85–108, 1988.

[13] R. Glowinski, T.W. Pan, T.I. Hesla, D.D. Joseph, and J. Périaux. A fictitious domain approach to the direct numerical simulation of incompressible viscous flow

past moving rigid bodies: Application to particulate flow. *Journal of Computational Physics*, 169:363–426, 2001.

[14] D. Kay, D. Loghin, and A. Wathen. A preconditioner for the steady-state Navier-Stokes equations. *SIAM J. Sci. Comput.*, 24(1):237–256, 2002.

[15] K.J. Bathe. *Finite Element Procedures*. Prentice Hall, Englewood Cliffs, N.J., 1996.

[16] K.J. Bathe and V. Sonnad. On effective implicit time integration in analysis of fluid-structure problems. *International Journal for Numerical Methods in Engineering*, 15:943–948, 1980.

[17] K.J. Bathe and H. Zhang. A flow-condition-based interpolation finite element procedure for incompressible fluid flows. *Computers & Structures*, 80:1267–1277, 2002.

[18] K.J. Bathe, H. Zhang, and S. Ji. Finite element analysis of fluid flows fully coupled with structural interactions. *Computers & Structures*, 72:1–16, 1999.

[19] K.J. Bathe, H. Zhang, and M.H. Wang. Finite element analysis of incompressible and compressible fluid flows with free surfaces and structural interactions. *Computers & Structures*, 56(2/3):193–213, 1995.

[20] H. Kohno and K.J. Bathe. A flow-condition-based interpolation finite element procedure for triangular grids. *International Journal for Numerical Methods in Fluids*, 49:849–875, 2005.

[21] S. Li and W.K. Liu. Reproducing kernel hierachical partition of unity part I: Formulation and theory. *International Journal for Numerical Methods in Engineering*, 45:251–288, 1999.

[22] M.D. Tidriri. Preconditioning techniques for the Newton-Krylov solution of compressible flows. *Journal of Computational Physics*, 132:51–61, 1997.

[23] R.J. LeVeque and Z.L. Li. Immersed interface methods for Stokes flow with elastic boundaries or surface tension. *SIAM Journal on Scientific Computing*, 18:709–735, 1997.

[24] Jr. R.P. Beyer. A computational model of the cochlea using the immersed boundary method. *Journal of Computational Physics*, 98:145–162, 1992.

[25] J.A. Sethian. *Level Set Methods and Fast Marching Methods*. Cambridge University Press, 1996.

[26] J.M. Stockie and B.R. Wetton. Analysis of stiffness in the immersed boundary method and implications for time-stepping schemes. *Journal of Computational Physics*, 154:41–64, 1999.

[27] T.E. Tezduyar. Stabilized finite element formulations for incompressible-flow computations. *Advances in Applied Mechanics*, 28:1–44, 1992.

[28] T.E. Tezduyar. Finite element methods for flow problems with moving boundaries and interfaces. *Archives of Computational Methods in Engineering*, 8:83–130, 2001.

[29] T.J.R. Hughes. *The finite element method: Linear static and dynamic analysis*. Prentice Hall, 1987.

[30] T.J.R. Hughes, L.P. Franca, and M. Balestra. A new finite element formulation for computational fluid dynamics: V. Circumventing the Babuška-Brezzi condition: A stable Petrov-Galerkin formulation of the Stokes problem accommodating equal-order interpolations. *Computer Methods in Applied Mechanics and Engineering*, 59:85–99, 1986.

[31] T.J.R. Hughes, W.K. Liu, and T.K. Zimmerman. Lagrangian-Eulerian finite element formulations for incompressible viscous flows. *Computer Methods in Applied Mechanics and Engineering*, 29:329–349, 1981.

[32] X. Wang. Finite element analysis of air-sheet interactions and flutter suppression devices. *Computers & Structures*, 64(5/6):983–994, 1997.

[33] X. Wang. Numerical analysis of moving orthotropic thin plates. *Computers & Structures*, 70:467–486, 1999.

[34] X. Wang. Velocity/Pressure mixed finite element and finite volume formulation with ALE descriptions for nonlinear fluid-structure interaction problems. *Advances in Engineering Software*, 31:35–44, 2000.

[35] X. Wang. Direct and iterative solution strategies using mixed finite element formulations with finite volume upwind and ALE descriptions for viscous fluids interacting with flexible structures. *SIAM Journal on Scientific and Statistical Computing*, 2006. submitted.

[36] X. Wang and W.K. Liu. Extended immersed boundary method using FEM and RKPM. *Computer Methods in Applied Mechanics and Engineering*, 193:1305–1321, 2004.

[37] X. Wang, W.K. Liu, and G. Chen. Immersed continuum method. *International Journal for Numerical Methods in Engineering*, 2004. Submitted.

[38] K. Washizu. *Variational Methods in Elasticity and Plasticity*. Pergamon, 1975.

[39] W.K. Liu, Y. Chen, C.T. Chang, and T.B. Belytschko. Advances in multiple scale kernel particle methods. *Computational Mechanics*, 18:73–111, 1996.

[40] W.K. Liu, S. Jun, and Y.F. Zhang. Reproducing kernel particle methods. *International Journal for Numerical Methods in Fluids*, 20:1081–1106, 1995.

[41] W.K. Liu and Y.J. Chen. Wavelet and multiple scale reproducing kernel methods. *International Journal for Numerical Methods in Fluids*, 21:901–932, 1995.

[42] Z.G. Feng, X. Wang, and E.E. Michaelides. A new approach to treat the solid-fluid boundary conditions in Lattice Boltzmann method. In *7th US National Congress on Computational Mechanics*, 2003.

[43] H. Zhang, X.L. Zhang, S.H. Ji, Y.H. Guo, G. Ledezma, N. Elabbasi, and H. deCougny. Recent development of fluid-structure interaction capabilities in the adina system. *Computers & Structures*, 81:1071–1085, 2003.

[44] L. Zhang, A. Gerstenberger, X. Wang, and W.K. Liu. Immersed finite element method. *Computer Methods in Applied Mechanics and Engineering*, 193:2051–2067, 2004.

[45] Z.J. Wang, J. Birch, and M. Dickinson. Unsteady forces and vorticity field in hovering flight: Two dimensional computations vs robotic wing experiments. *J. Exp. Biol.*, 207:449–460, 2004.